Ligand effect on the kinetics of hydroperoxochromium(III)–oxochromium(V) transformation and the lifetime of chromium(V)†

Kelemu Lemma, Arkady Ellern and Andreja Bakac*

Received 3rd August 2005, Accepted 12th October 2005
First published as an Advance Article on the web 28th October 2005
DOI: 10.1039/b511084j

A macrocyclic superoxochromium complex $L^2(H_2O)CrOO^{2+}$ (L^2 = *meso*-Me_6-[14]aneN_4) is generated from $L^2Cr(H_2O)_2^{2+}$ and O_2 with $k_{on} = (2.80 \pm 0.07) \times 10^7$ M^{-1} s^{-1}. One-electron reduction of $L^2(H_2O)CrOO^{2+}$ produces a transient hydroperoxo complex that readily undergoes intramolecular conversion to $L^2Cr(V)$, $k_1 = 1.00 \pm 0.01$ s^{-1} in acidic aqueous solutions, and 0.273 ± 0.010 s^{-1} at pH >7, with an apparent pK_a of 5.9. The decay of $L^2Cr(V)$ in the pH range 1.3–6.2 obeys the rate law, $-d[L^2Cr(V)]/dt = (0.0080 (\pm 0.0049) + 8.19 (\pm 0.13)\ [H^+])[L^2Cr(V)]$. Both the kinetics of formation and lifetime of $L^2Cr(V)$ are significantly different from those for the closely related [14]aneN_4 complex. The X-ray structure of the parent Cr(III) complex, $[L^2Cr(H_2O)_2](ClO_4)_3 \cdot 4H_2O$, shows that the macrocyclic ligand adopts the most stable, "two up-two down" configuration around the nitrogens.

Introduction

The reaction between $L^1Cr(H_2O)_2^{2+}$ (L^1 = cyclam, or [14]aneN_4) and molecular oxygen generates intermediates whose chemistry in many respects resembles that observed for cytochrome P450 enzymes.[1–3] Previously, we have studied the formation and reactivity of the chromium intermediates, and characterized them spectroscopically and kinetically.[4–6] Undoubtedly, the most intriguing reaction is the facile and rapid intramolecular conversion of the hydroperoxochromium(III) complex to $L^1Cr(V)$. Such transformations are not only a mechanistic curiosity; there is a realistic possibility that such chemistry might provide a way for "innocent" chromium(III) complexes in biological environments to be converted to higher, carcinogenic oxidation states,[7] Cr(V) and ultimately Cr(VI).[8]

Somewhat unexpectedly, there is no kinetic dependence on [H^+] for this step[5] for either of the two hydrolytic forms of the hydroperoxo complex, $L^1(H_2O)CrOOH^{2+}$ and $L^1(HO)CrOOH^+$, which are related by a pK_a of 5.6, eqn (1)–(3).

$$L^1(H_2O)CrOOH^{2+} \rightleftharpoons L^1(HO)CrOOH^+ + H^+ : pK_a = 5.6 \quad (1)$$

$$L^1(H_2O)CrOOH^{2+} \rightarrow L^1(OH)Cr^VO^{2+} + H_2O : k = 0.191\ s^{-1} \quad (2)$$

$$L^1(OH)CrOOH^{2+} \rightarrow L^1Cr^V(O)_2^+ + H_2O : k = 0.025\ s^{-1} \quad (3)$$

We have now turned to another chromium complex, $L^2(H_2O)_2Cr^{2+}$ (L^2 = Me_6-[14]aneN_4). Chemically and structurally, L^1 and L^2 are closely related, but the change of the macrocyclic ligand was expected to influence the kinetics of various steps, and, ideally, increase the lifetime of some intermediates to allow more detailed spectroscopic and mechanistic studies. Such effects have precedents in the cobalt and rhodium chemistry. In both cases, the L^2 superoxo complexes homolyze much more readily than the L^1 analogues.[9,10] We expected the opposite effect on the lifetime of Cr(V), which should derive extra stability from electron donation by the methyl groups of L^2.

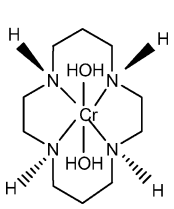

$L^1(H_2O)_2Cr^{2+}$

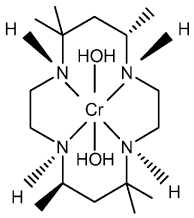

$L^2(H_2O)_2Cr^{2+}$

Experimental

C-*meso*-Me_6-1,4,8,11-tetraazacyclotetradecane (L^2) and $[L^2CrCl_2]Cl$ were prepared according to literature methods.[11,12] The purity of the prepared samples was checked by ^1H NMR (ligand) and UV-Vis spectroscopy (metal complex). The ethylchromium complex, $L^2(H_2O)CrCH_2CH_3^{2+}$, was prepared from the Cr(II) precursor and *tert*-amylhydroperoxide by a procedure reported earlier for the L^1 analogue, and purified by ion exchange on Sephadex C-25. Commercial samples of $[Ru(NH_3)_6]Cl_3$, $(NH_4)_2ABTS$ ($ABTS^{2-}$ = 2,2′-azino-bis(ethylbenzothiazoline-6-sulfonate)), both Aldrich, 2-(*N*-morpholino)-ethanesulfonic acid (MES), piperazine-*N*,*N*′-bis(4-butanesulfonic acid) (PIPBS), both GFS chemicals, were used as received. Other chemicals were of reagent grade or better. Acidic stock solutions of $L^2Cr(H_2O)_2^{3+}$ (21–64 mM) were prepared by a method described earlier for the L^1 complex.[13] A suspension of 1.0 g of $[L^2CrCl_2]Cl$ in 500 mL of 15 mM CF_3SO_3H was reduced on zinc amalgam in an argon atmosphere. When all the material dissolved, the amalgam was removed, and oxygen was passed through the solution to oxidize $L^2Cr(H_2O)_2^{2+}$ to $L^2Cr(H_2O)_2^{3+}$. The complex was purified by ion exchange on Sephadex C-25 and eluted with 1.0 M CF_3SO_3H.

Chemistry Department, Iowa State University of Science and Technology, Ames, IA, 50011, USA. E-mail: bakac@ameslab.gov

† Electronic supplementary information (ESI) available: Fig. S1–S5. See DOI: 10.1039/b511084j

Stock solutions of $L^2Cr(H_2O)_2^{2+}$ were prepared by zinc amalgam reduction of $L^2(H_2O)_2Cr^{3+}$ under argon. Fresh stock solutions of $L^2(H_2O)CrOO^{2+}$ were prepared daily by injecting small amounts of $L^2Cr(H_2O)_2^{2+}$ into oxygen-saturated solutions of dilute (1–50 mM) $HClO_4$ or CF_3SO_3H, and kept under oxygen in an ice bath. Stock solutions of $Ru(NH_3)_6^{3+}$ (10 mM) and $ABTS^{2-}$ (20 mM) were prepared in dilute $HClO_4$ and stored under argon.

The acidity of kinetic solutions was maintained with $HClO_4$ and CF_3SO_3H at pH < 3, and with MES and PIBPS buffers at pH >3. Laboratory-distilled water was further purified by passage through a Millipore Milli Q water purification system. Unless noted otherwise, the kinetic data are given at 25 ± 0.2 °C and 0.10 M ionic strength.

Most kinetic experiments used an Olis RSM 1000 stopped-flow apparatus. Kinetic data were collected by rapid scanning (Δt = 1 ms) in the range 336–562 nm. A Shimadzu 3101 PC UV-VIS spectrophotometer was used for slow kinetics and for UV-Vis spectral measurements. Data were analyzed with OLIS GlobalWorks v2.0.190 and KaleidaGraph 3.6 PC software. pH measurements utilized a Corning 320 pH meter.

The kinetics of O_2 binding to $L^2Cr(H_2O)_2^{2+}$ were determined by laser flash photolysis of $L^2(H_2O)CrCH_2CH_3^{2+}$ in oxygenated solution, λ_{exc} 266 nm. The photochemical event generates ethyl radicals and $L^2Cr(H_2O)_2^{2+}$. The reaction of the latter with O_2 was monitored at 293 nm, an absorption maximum for $L^2(H_2O)CrOO^{2+}$ ($\varepsilon = 3.0 \times 10^3$ M^{-1} cm^{-1}).

ESR spectra were obtained on frozen samples (T = 115 K) at pH 2.0 and 4.3 with a Bruker ER 200 D-SRC spectrometer. Solutions of L^2Cr(V), prepared from equimolar amounts of $L^2(H_2O)CrOO^{2+}$ and $Ru(NH_3)_6^{2+}$, were mixed with an equal volume of propylene glycol, transferred into ESR tubes and frozen to a glass in liquid nitrogen. After the completion of data collection, the samples were warmed up to room temperature to allow L^2Cr(V) to decompose, and the spectrum was recorded again at 115 K. The difference between the spectra of fresh and decomposed samples is shown in the Results. The spectra were run again on a new set of solutions containing 2,2-diphenyl-1-picrylhydrazyl (DPPH) in addition to L^2Cr(V). The g value for L^2Cr(V) was obtained relative to g = 2.0036 for DPPH.

Crystal structure of $[L^2(H_2O)_2Cr](ClO_4)_3 \cdot 4H_2O$

A solution of $L^2(H_2O)_2Cr^{3+}$ in dilute $HClO_4$ was allowed to evaporate slowly at room temperature. Single crystals for crystal structure determination were obtained within a week. The data collection (at 193 K) and structure determination were undertaken in the usual way.

A pink crystal with approximate dimensions 0.3 × 0.1 × 0.1 mm of $[L^2(H_2O)_2Cr](ClO_4)_3 \cdot 4H_2O$: $C_{16}H_{44}Cl_3CrN_4O_{18}$, T = 193 K: monoclinic, space group $P2_1/c$, Z = 4, a = 8.7575(15), b = 20.964(4), c = 17.009(3) Å, β = 99.195(3)°, V = 3082.5(9) Å^3, D_c = 1.592 Mg m^{-3}, μ = 0.712 mm^{-1}, $F(000)$ = 1548. X-Ray intensity data were measured on a Bruker SMART CCD 1000™ diffractometer [$\lambda_{MoK\alpha}$ = 0.711069 Å, graphite monochromator, a scan width of 0.3° in ε and exposure time of 10 s frame^{-1}, detector–crystal distance 5.03 cm]. A full sphere algorithm and narrow-frame integration lead to a total of 25436 reflections (θ < 26.43°), of which 6284 reflections were independent (R_{int} = 0.0856) and 4676 with $F_o > 4\sigma(F_o)$. Data were corrected for absorption using Bruker SADABS (Bruker Analytical X-Ray Systems, Madison, WI, USA, 2001) program. The structure was solved by direct methods and refined by least squares in full-matrix approximation. Hydrogen atoms of the cyclam ligand were placed in calculated positions and refined using the "riding model'. H-atoms of the ligand water and solvent water were not located and were not included in the refinement. The structure was refined (385 parameters) to $R1$ = 0.0947, $wR2$ = 0.2597, GOF = 1.047. The SHELXTL version 5.1 (Bruker Analytical X-Ray Systems, Madison, WI, USA, 2001) software package was used for calculations and drawings.

CCDC reference number 279794.

For crystallographic data in CIF or other electronic format see DOI: 10.1039/b511084j

Results

The ORTEP diagram of the cation *trans*-$L^2Cr(H_2O)_2^{3+}$ is shown in Fig. 1. Selected bond distances and angles are listed in Table 1.

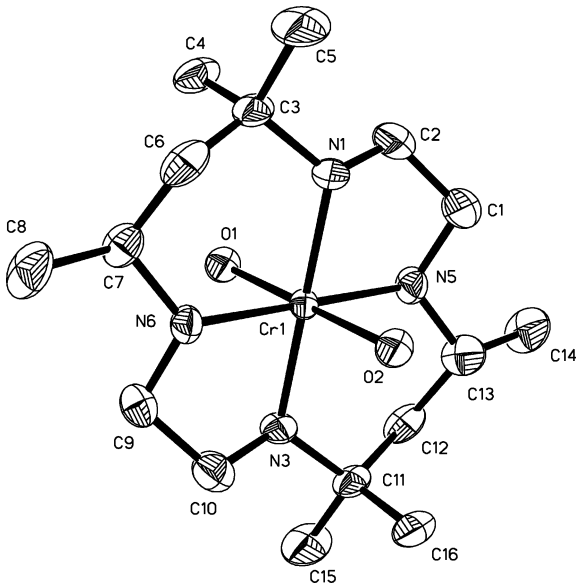

Fig. 1 ORTEP drawing of the molecular structure of the cation *trans*-$L^2Cr(H_2O)_2^{3+}$ (L^2 = *C-meso*-Me_6-1,4,8,11-tetraazacyclotetradecane) with H-atoms omitted for clarity. Thermal ellipsoids are drawn at the 50% probability level.

Table 1 Selected bond distances (Å) and bond angles (°) for *trans*-$[L^2Cr(H_2O)_2](ClO_4)_3 \cdot 4H_2O$

Cr(1)–O(1)	2.008(4)	Cr(1)–N(3)	2.061(4)
Cr(1)–O(2)	2.009(4)	Cr(1)–N(5)	2.042(5)
Cr(1)–N(1)	2.075(4)	Cr(1)–N(6)	2.051(4)
N(1)–Cr(1)–N(3)	179.67(19)	O(1)–Cr(1)–N(3)	88.03(17)
N(1)–Cr(1)–N(5)	84.80(19)	O(1)–Cr(1)–N(5)	89.03(18)
N(1)–Cr(1)–N(6)	94.83(18)	O(1)–Cr(1)–N(6)	91.32(17)
N(3)–Cr(1)–N(5)	95.31(18)	O(2)–Cr(1)–N(1)	87.64(17)
N(3)–Cr(1)–N(6)	85.06(18)	O(2)–Cr(1)–N(3)	92.04(17)
N(5)–Cr(1)–N(6)	179.50(19)	O(2)–Cr(1)–N(5)	90.82(18)
O(1)–Cr(1)–O(2)	179.83(17)	O(2)–Cr(1)–N(6)	88.84(17)
O(1)–Cr(1)–N(1)	92.29(17)		

The geometry around the chromium is octahedral with two water molecules in the axial positions. The four equatorial sites are occupied by the nitrogen atoms of the macrocycle in the thermodynamically most stable "two up-two down" (*R*,*R*,*S*,*S*) configuration. The chromium atom is coplanar with the four nitrogen atoms (RMS = 0.0023 Å). No intermolecular interactions related to N atoms have been observed as the shortest N···O distances exceed 3 Å. The shortened "water ligands–water solvent" intermolecular O···O distances (all exceed 2.58 Å) were observed. This can indicate a weak intermolecular interaction in the solid state between the cluster and water ligands, but those distances are too long for strong hydrogen bonding. The typical disorder of highly symmetrical perchlorate anions has resulted in comparatively large values of *R*-factors and thermal displacement coefficients for oxygen atoms.

ESR spectra at pH 2 and pH 4.3 are shown in Fig. 2. The two spectra have identical *g* values, 2.0024, calibrated against DPPH (g 2.0036). The spectrum at pH 4.3 is, however, broader and has an additional feature that is not found at pH 2.

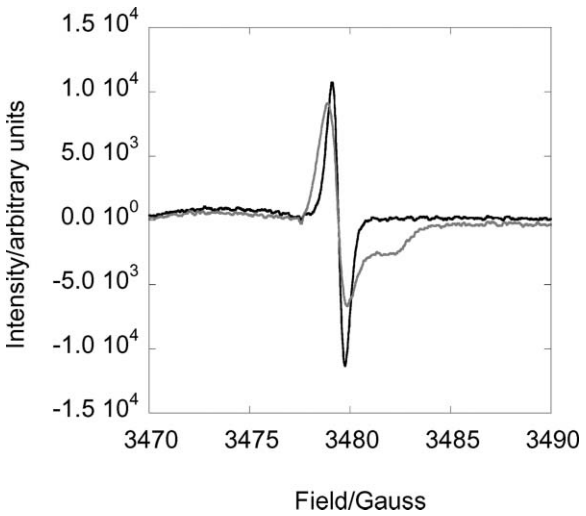

Fig. 2 Difference ESR spectra between the fresh and decomposed samples of $L^2Cr(v)$ at pH 2.0 (black) and 4.3 (grey) in 1 : 1 (v/v) water–propylene glycol glass at 115 K. Instrument settings: center field 3400 G, sweep width 800 G, microwave frequency ~4.7 GHz, modulation 12.5, receiver gain 1.25×10^5, time constant 100 ms, 25 scans.

Kinetics of O_2 binding

Laser flash photolysis experiments were carried out at three different O_2 concentrations in 0.60 M CF_3SO_3H. A linear plot of k_{obs} *vs.* $[O_2]$ (Fig. S1, ESI†) gave $k_{on} = (2.80 \pm 0.07) \times 10^7$ M^{-1} s^{-1}, eqn (4).

$$L^2Cr(H_2O)_2^{2+} + O_2 \underset{k_{off}}{\overset{k_{on}}{\longleftrightarrow}} L^2(H_2O)CrOO^{2+} + H_2O \qquad (4)$$

Reaction of $L^2(H_2O)CrOO^{2+}$ with reductants

Guided by our previous experience with $L^1(H_2O)CrOOH^{2+}$, we determined the rate constants k_{CrOO}, k_1 and k_2 in the reactions with $Ru(NH_3)_6^{2+}$ and $ABTS^{2-}$ according to Scheme 1.

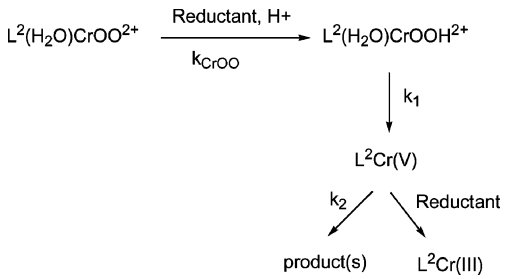

Scheme 1

The reaction of 8×10^{-5} M $L^2(H_2O)CrOO^{2+}$ with an equimolar amount of $Ru(NH_3)_6^{2+}$ at 3×10^{-6} –0.054 M H^+ was monitored at 270–415 and 375–523 nm as a function of $[H^+]$ and temperature. The initial redox step was too fast for precise kinetic determinations, and only an estimate was obtained, $k_{CrOO} \sim 10^6$ M^{-1} s^{-1}. The observed kinetic traces were biphasic, Fig. 3, and yielded the rate constants for the formation (k_1) and decay (k_2) of $L^2Cr(v)$. These experiments also yielded UV-Vis spectral data for the intermediate $L^2Cr(v)$, Fig. 4. The assignment of the specific rate

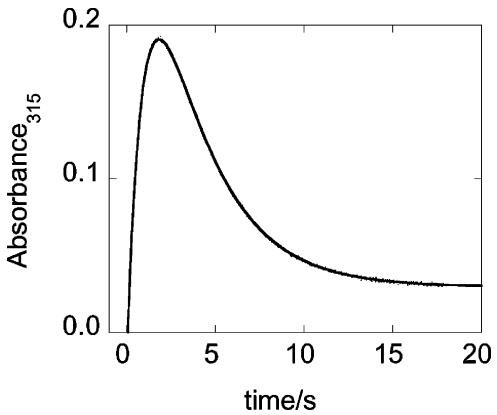

Fig. 3 Kinetic curve and the biexponential fit for the formation and decay of $L^2Cr(v)$ generated from 6.4×10^{-5} M $L^2(H_2O)CrOO^{2+}$ and 7.0×10^{-5} M $Ru(NH_3)_6^{2+}$ at 0.035 M H^+.

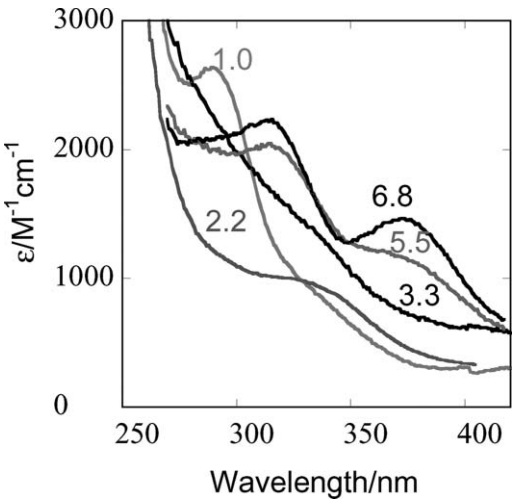

Fig. 4 UV spectra of $L^2Cr(v)$, derived from biexponential stopped-flow traces at pH 1.0, 2.2, 3.3, 5.5 and 6.8.

constants to the individual steps in Scheme 1 was confirmed in experiments with $ABTS^{2-}$, as described later.

The rate constant k_1 exhibited a titration-type behavior, as shown in Fig. 5. The limiting values are $k_{1a} = 1.00 \pm 0.01\ s^{-1}$ (acidic range) and $k_{1b} = 0.273 \pm 0.010\ s^{-1}$ (pH > 7). The data were fitted to eqn (5) to yield the acid dissociation constant for $L^2(H_2O)CrOOH^{2+}$, $pK_a = 5.9$ (eqn (6)).

$$k_{obs} = \frac{k_{1a}[H^+] + k_{1b}K_a}{[H^+] + K_a} \quad (5)$$

$$L^2(H_2O)CrOOH^{2+} \rightleftharpoons L^2(HO)CrOOH^{+} + H^+ \quad (6)$$

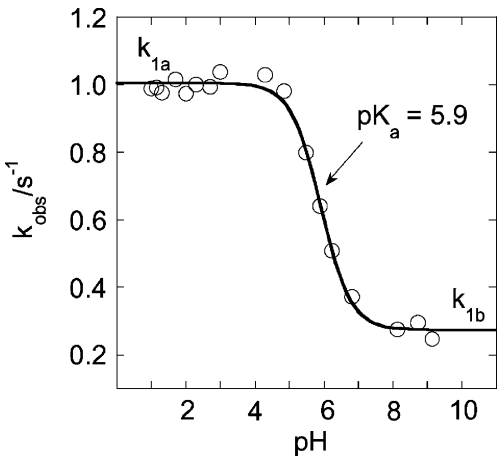

Fig. 5 Plot of k_{obs} *vs.* pH for the transformation of $L^2(H_2O)CrOOH^{2+}$ to $L^2Cr(v)$ at 25 °C.

The kinetics of $L^2Cr(v)$ decay were exponential in the pH range 1–6, although some tailing at longer times was observed at pH > 5. The dependence on pH is shown in Fig. 6, which also shows a plot of k_{obs} against $[H^+]$. This plot is linear with a slope of $8.19 \pm 0.13\ M^{-1}\ s^{-1}$ and an intercept of $0.0080 \pm 0.0049\ s^{-1}$.

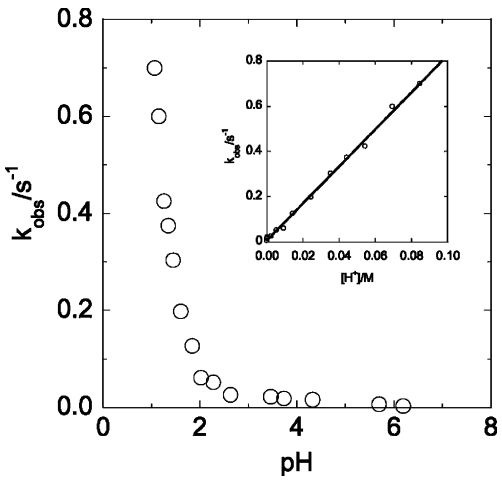

Fig. 6 Plot of k_{obs} *vs.* pH for the decay of $L^2Cr(v)$. Inset: plot of k_{obs} *vs.* $[H^+]$.

The temperature dependence of the rate constants k_1 and k_2 is shown in the Eyring plots in Fig. S2 and S3 (ESI†).

The reaction between $L^2(H_2O)CrOO^{2+}$ and $ABTS^{2-}$ in 0.020 M $HClO_4$ yielded single exponential traces in the limits of low (<0.04 mM) and high (>0.15 mM) concentrations of $ABTS^{2-}$, but appeared biphasic in the intermediate regime. Under all the conditions, the reaction generated three equivalents of $ABTS^{\bullet-}$ for each mole of $L^2(H_2O)CrOO^{2+}$ consumed. At low $[ABTS^{2-}]$, the rate constants were $[ABTS^{2-}]$-dependent and yielded an estimate for k_{CrOO} of *ca.* $2 \times 10^4\ M^{-1}\ s^{-1}$, Fig. S4 (ESI†).

At high $[ABTS^{2-}]$, the redox step was completed in mixing time and produced one equivalent of $ABTS^{\bullet-}$. The initial absorbance jump was followed by a first-order absorbance increase that generated two more equivalents of $ABTS^{\bullet-}$ and had a rate constant $k_1 = 1.00 \pm 0.01\ s^{-1}$, independent of $[ABTS^{2-}]$ and identical to that observed for one of the stages in the $Ru(NH_3)_6^{2+}$ reaction. The lack of dependence on $[ABTS^{2-}]$ defines this step as k_1, followed by a rapid reduction of a newly formed $L^2Cr(v)$ by two more equivalents of $ABTS^{2-}$. The biphasic behavior at the intermediate concentrations of $ABTS^{2-}$ is easily understood by the gradual change of rate determining step from k_{CrOO} to k_1.

The initial redox step between $L^2(H_2O)CrOO^{2+}$ and $ABTS^{2-}$, measurable only at very low $[ABTS^{2-}]$, see above, is acid catalyzed at low $[H^+]$, but reaches a constant value at about 0.1 M H^+, Fig. 7. Both reactants can be protonated in the acidity range examined, and the saturation in Fig. 7 must result from the cancellation of two opposing acid/base equilibria, see Discussion.

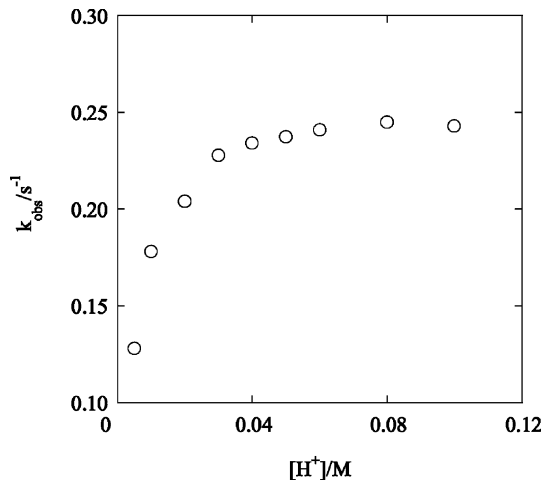

Fig. 7 Plot of k_{obs} *vs.* $[H^+]$ for the reduction of L^2CrOO^{2+} (0.6 μM) with $ABTS^{2-}$ (10 μM).

The reaction between $L^2(H_2O)CrOO^{2+}$ and iodide was examined briefly in the acidity range $0.005 \leq [H^+] \leq 0.030$ M. The absorbance increase at 351 nm (I_3^-) obeyed the mixed third-order rate law of eqn (7), and yielded $k_I = 729 \pm 13\ M^{-2}\ s^{-1}$. The data are shown in Fig. S5 (ESI†). All the kinetic data are summarized in Table 2.

$$-d[L^2(H_2O)CrOO^{2+}]/dt = k_I[H^+][I^-][L^2(H_2O)CrOO^{2+}] \quad (7)$$

Discussion

The chemistry and intermediates involved in the $L^2Cr(H_2O)_2^{2+}/O_2$ reaction for the most part follow closely those observed for the L^1 analogue. This includes the rapid initial O_2 capture to generate $L^2(H_2O)CrOO^{2+}$, and its facile reduction to $L^2(H_2O)CrOOH^{2+}$ followed by intramolecular conversion to a Cr(v) complex. The

Table 2 Summary of kinetic and thermodynamic data for the reactions of macrocyclic chromium complexes with O_2[a]

	Reaction	$L = L^2$	$L = L^1$	Conditions	Source[b]
k_{on}	$L(H_2O)_2Cr^{2+}/O_2$	2.80 (± 0.07) × 10^7	1.80 (± 0.06) × 10^8	20 mM H^+	4
k_{CrOO}	$L(H_2O)CrOO^{2+}/Ru(NH_3)_6^{2+}$	>2 × 10^6	7.0 (± 0.1) × 10^4	20 mM H^+	4
k_{CrOO}	$L(H_2O)CrOO^{2+}/ABTS^{2-}$	~2 × 10^4	2.5 × 10^4	20 mM H^+	4
k_{1a}	$L(H_2O)CrOOH^{2+} \rightarrow LCr(v)$ [c]	1.00 (± 0.01) s[d]	0.18 (± 0.01)[d]	pH 1–4	5
$\Delta H^{\ddagger}_{1a}$		63.1 (± 0.8)	53.7 (± 7.3)		
$\Delta S^{\ddagger}$		−33.1 (± 2.7)	−80.5 (± 24.0)		
k_{1a}	$L(H_2O)CrOOH^{2+} \rightarrow LCr(v)$[e]	1.00 (± 0.02)[d]	0.17 (± 0.01)[d]	pH 1–3	5
k_{1b}	$L(OH)CrOOH^{2+} \rightarrow LCr(v)$[c]	0.273 (± 0.010)[d]	0.025 (± 0.003)[d]	pH > 7	5
$\Delta H^{\ddagger}_{1b}$		62.7 (± 1.3)			
$\Delta S^{\ddagger}_{1b}$		−44.4 (± 4.3)			
pK_a	$L(H_2O)CrOOH^{2+} \rightleftharpoons L(HO)CrOOH^+$	5.9 (± 0.1)	5.6 (± 0.1)	pH 1–7	5
k_2	$LCr(v) \rightarrow$ products[c]	8.06 (± 0.23) $[H^+]$ + 0.0080(± 0.0049)	0.416 (± 0.008)[d]	pH 1–2	5
$\Delta H^{\ddagger}_2$		43.7 (± 1.4)	57.2 (± 4.5)		
$\Delta S^{\ddagger}_2$		−108 (± 5)	−59.7 (± 14.6)		
k_I	$L(H_2O)CrOO^{2+}/I^-$	729 (± 13)[f]	402 (± 7)[f]	5–30 mM H^+	14

[a] At 25.0 ± 0.2° C; L^1 = [14]aneN$_4$; L^2 = Me_6-[14]aneN$_4$. Units: k/M^{-1} s^{-1}, $\Delta H^{\ddagger}$/kJ mol, $\Delta S^{\ddagger}$/J mol^{-1} K^{-1}). Numbers in parentheses represent one standard deviation. [b] For $L = L^1$. [c] $Ru(NH_3)_6^{2+}$ used as reductant for $L(H_2O)CrOO^{2+}$. [d] Units: s^{-1}. [e] $ABTS^{2-}$ used as reductant for $L(H_2O)CrOO^{2+}$. [f] Units: M^{-2} s^{-1}.

kinetic data for various steps are shown for both series of complexes in Table 2.

The greatest difference between the two series was observed at the Cr(v) stage. The rate constant k_1 for the formation of $L^2Cr(v)$ is ~5 times larger than that for the L^1 complex, and the decay rate constant k_2 is under most conditions lower for $L^2Cr(v)$. This behavior is consistent with L^2 providing greater stabilization to the Cr(v) state, which is easily explained by the electron donation from the peripheral methyl groups.

The rate constant k_1 follows the same general pattern for both hydroperoxides, *i.e.* the reaction displays a titration-type behavior, as shown for $L^2Cr(v)$ in Fig. 5. As discussed in detail earlier,[5] this somewhat unexpected result and lack of direct acid catalysis suggest a formal intramolecular proton shift from coordinated water to the hydroperoxo group to create the pull–push effect and "turn on" the intramolecular electron transfer and simultaneous dissociation of a molecule of water to generate $L^2Cr(v)$. The negative entropies of activation reflect the tightening of both first and second coordination spheres around the metal as the oxidation state increases. The pK_a values for the two hydroperoxo complexes are comparable, 5.9 *vs.* 5.6. The somewhat larger value for the L^2 complex is as expected from the increased basicity of the L^2 ligand.

The decay of the two Cr(v) complexes follows different patterns. $L^1Cr(v)$ exhibits two limiting first order rate constants (0.416 s^{-1} and 0.103 s^{-1}) and a pK_a of 4.9.[5] The decay of $L^2Cr(v)$, on the other hand, is dominated by a term that is first order in $[H^+]$ at high $[H^+]$, and exhibits an acid independent term measurable at $[H^+] < 3$ mM.

On the basis of spectral and charge data we suggested previously that $L^1(OH)CrO^{2+}$ and $L^1Cr(O)_2^+$, related by a pK_a of 4.9,[5] are the dominant forms of $L^1Cr(v)$ in acidic solutions. The UV-Vis spectrum (Fig. 2) of $L^2Cr(v)$ suggests that there is an additional form, most likely $L^2(H_2O)CrO^{3+}$, present in strongly acidic solutions of the L^2 complex. The dramatic change in the UV-Vis spectrum as the pH increases from 1 to 2 coincides with the large decrease in k_2, Fig. 6. The linear dependence of k_2 on $[H^+]$ requires that $pK_a < 1$ for $L^2(H_2O)CrO^{3+}/L^1(OH)CrO^{2+}$. The aqua-oxo form, $L^2(H_2O)CrO^{3+}$, decays much more readily than any of the other hydrolytic forms and completely dominates the kinetics at $[H^+] > 3$ mM. The reactivity of other form(s) is represented by the intercept in the inset in Fig. 6, although the precision of the fitted parameter is low, k = (0.0080 ± 0.0049 s^{-1}). Much more convincing are the experimental rate constants which are much larger than calculated for the acid dependent path at pH >3. The measured values of 0.016–0.022 s^{-1} in the pH range 3.5–4.5 are 5–40 times greater than those calculated for the acid-catalyzed path. Clearly, the more hydrolyzed forms, $L^1(OH)CrO^{2+}$ and $L^2Cr(O)_2^{3+}$ also decompose, although the small rate constants combined with the eventual departure from exponential kinetics has thwarted our efforts to determine the pK_a relating these two forms. For the L^1 complex, the pK_a is 4.9.[5]

The kinetic and spectral evidence obtained for $L^2(H_2O)CrO^{3+}$ at pH 1–2 stands in contrast with the corresponding data for the L^1 complex, for which the decay rate constant k = 0.41 s^{-1} remained unchanged in the pH range 1–4. Qualitatively, the trend is as expected on the basis of the greater electron-donating ability of L^2, but it is surprising that the effect is so much greater at the Cr(v) level than for the Cr(III) hydroperoxo complexes where the acidity constants of the L^1 and L^2 species differ by only a factor of two, Table 2.

Despite the clear differences in rate laws, complexes $L^1Cr(v)$ and $L^2Cr(v)$ both decay faster at higher $[H^+]$, as expected if an oxo or hydroxo chromium(v) is reduced to aqua chromium(III). Although work with low concentrations has prevented us from isolating the products of Cr(v) decay for either macrocycle, we believe that the reaction is initiated by an intramolecular electron transfer to yield a Cr(III) complex of modified (oxidized) macrocycle. The other, much less likely option that involves the loss of macrocycle and disproportionation of the metal is ruled out by the absence of $HCrO_4^-$ among the products.

Some increase in the rate of formation, and increased stability of $L^2Cr(V)$ as compared to $L^1Cr(V)$ was to be expected on electronic grounds. Still, the two complexes are very much alike and yet the observed kinetic differences are significant. In a biological milieu, a number of potential ligands are available to chromium, and it is plausible that some of them may facilitate the chemistry of the type shown in eqn (1)–(3), as suggested by other authors.[16]

In our earlier work, we have presented evidence that superoxometal complexes become more powerful oxidants upon protonation, although the protonated forms eluded spectroscopic detection, probably because $L(H_2O)CrOOH^{3+}$ ($L = (H_2O)_4$ and L^1) is only a minor species even at the highest acid concentrations used.[14] The kinetic evidence was, however, convincing. The reductants selected for those experiments (I^-, Br^-, $(NH_3)_5Ru(py)^{2+}$) do not participate in acid–base equilibria under experimental conditions, which leaves the superoxo complexes as the only reasonable proton acceptors and thus the source of the observed acid dependence. The oxidation of I^- by $L^2(H_2O)CrOO^{2+}$ in this work follows the same pattern and has a rate constant that is somewhat larger than that for the L^1 complex.

Another reductant chosen in this work, $ABTS^{2-}/HABTS^-$, has $pK_{a,A} = 2.2$.[17] Of the two forms, $ABTS^{2-}$ is the more reducing.[17] On these grounds, it is reasonable to expect that the reactive species in the present case would be $L^2(H_2O)CrOOH^{3+}$ and $ABTS^{2-}$, as shown in eqn (8)–(10).

$$L^2(H_2O)CrOOH^{2+} \rightleftharpoons L^2(H_2O)CrOO^{2+} + H^+ : K_{a,Cr} \quad (8)$$

$$HABTS^- \rightleftharpoons ABTS^{2-} + H^+ : K_{a,A} \quad (9)$$

$$L^2(H_2O)CrOOH^{3+} + ABTS^{2-} \xrightarrow{k_{10}} L^2(H_2O)CrOOH^{2+} + ABTS^- \quad (10)$$

After introducing the inequality $K_{a,Cr} \gg [H^+]$, the rate law in eqn (11) is derived, where $[ABTS^{2-}]_{av}$ represents the sum $\{[ABTS^{2-}] + [HABTS^-]\}$. The fit of the data to eqn (11) is shown in Fig. 8 and yields $k_{10}/K_{a,Cr} = (3.56 \pm 0.04) \times 10^6\ M^{-2}\ s^{-1}$. The excellent linearity of the plot in Fig. 8 places a limit on $K_{a,Cr}$ at > 1 M which in turn requires that k_{10} be greater than $10^6\ M^{-1}\ s^{-1}$, a reasonable value for a reaction with a large driving force (>0.3 V) and a large self-exchange rate constant for at least one reactant, $ABTS^{2-}/ABTS^{\bullet -}$.

$$\frac{k_{obs}(K_{a,A} + [H^+])}{[ABTS^{2-}]_{av} K_{a,A}} = \frac{k_{10}[H^+]}{K_{a,Cr}} \quad (11)$$

The $[H^+]$ dependence of the $L^2(H_2O)CrOO^{2+}/ABTS^{2-}$ reaction provides strong support for the existence and reactivity of the so far unobserved protonated form, $L^2(H_2O)CrOOH^{3+}$.

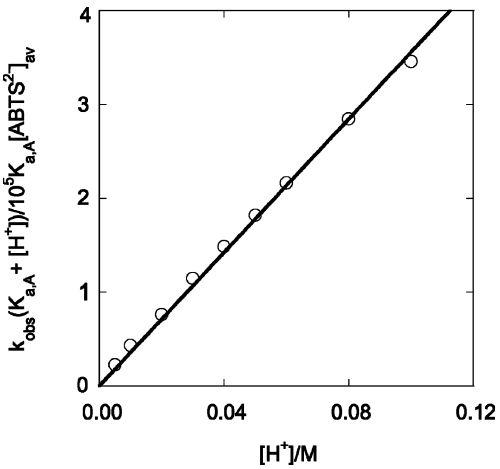

Fig. 8 Plot according to eqn (11) for the reaction between $L^2(H_2O)CrOO^{2+}$ and $ABTS^{2-}$.

The rate constant k_{on} for oxygen binding to $L^2Cr(H_2O)_2^{2+}$, $2.80 \times 10^7\ M^{-1}\ s^{-1}$, is somewhat smaller than the value for the L^1 complex. The same pattern, believed to be determined by steric factors, was observed earlier for the Co complexes of the same ligands.[9]

Acknowledgements

This work was supported by a grant from the National Science Foundation, CHE 0240409. Some of the work was conducted with the use of facilities at the Ames Laboratory.

References

1 A. Bakac, *Prog. Inorg. Chem.*, 1995, **43**, 267–351.
2 A. Bakac, *Adv. Inorg. Chem.*, 2004, **55**, 1–59.
3 P. R. O. De Montellano and J. J. De Voss, *Nat. Prod. Rep.*, 2002, **19**, 477–493.
4 A. Bakac and W.-D. Wang, *Inorg. Chim. Acta*, 2000, **297**, 27–35.
5 O. Pestovsky and A. Bakac, *Dalton Trans.*, 2005, 556–560.
6 O. Pestovsky and A. Bakac, *J. Am. Chem. Soc.*, 2003, **125**, 14714–14715.
7 R. P. Farrell, R. J. Judd, P. A. Lay, N. E. Dixon, R. S. U. Baker and A. M. Bonin, *Chem. Res. Toxicol.*, 1989, **2**, 227–229.
8 A. Levina and P. A. Lay, *Coord. Chem. Rev.*, 2005, **249**, 281–298.
9 A. Bakac and J. H. Espenson, *J. Am. Chem. Soc.*, 1990, **112**, 2273–2278.
10 O. Pestovsky and A. Bakac, *J. Am. Chem. Soc.*, 2002, **124**, 1698–1703.
11 R. W. Hay and G. A. Lawrance, *J. Chem. Soc., Perkin Trans. 1*, 1975, 591–593.
12 D. A. House, R. W. Hay and M. A. Ali, *Inorg. Chim. Acta*, 1983, **72**, 239–245.
13 A. Bakac, V. Butkovic, J. H. Espenson and M. Orhanovic, *Inorg. Chem.*, 1993, **32**, 5886–5888.
14 A. Bakac, C. Shi and O. Pestovsky, *Inorg. Chem.*, 2004, **43**, 5416–5421.
15 O. Pestovsky and A. Bakac, *Inorg. React. Mech.*, 2005, **5**, 245–254.
16 R. Codd, C. T. Dillon, A. Levina and P. A. Lay, *Coord. Chem. Rev.*, 2001, **216–217**, 537–582.
17 S. L. Scott, W.-J. Chen, A. Bakac and J. H. Espenson, *J. Phys. Chem.*, 1993, **97**, 6710–6714.